Piezo1 mechanosensing regulates integrin-dependent chemotactic migration in human T cells

Chinky Shiu Chen Liu[1], Tithi Mandal[2], Parijat Biswas[3], Md. Asmaul Hoque[1,4], Purbita Bandopadhyay[1,4], Bishnu Prasad Sinha[1,4], Jafar Sarif[1,4], Ranit D'Rozario[1,4], Deepak Kumar Sinha[3], Bidisha Sinha[2], Dipyaman Ganguly[1]*

[1]IICB-Translational Research Unit of Excellence, CSIR-Indian Institute of Chemical Biology, Kolkata, India.

[2]Department of Biological Sciences, Indian Institute of Science Education and Research, Kolkata, India.

[3] Department of Biological Sciences, Indian Association for Cultivation of Science, Kolkata, India.

[4]Academy of Scientific and Innovative Research, Ghaziabad, India.

Correspondence: dipyaman@iicb.res.in

Running title: Piezo1 mechanosensing in human T cell chemotaxis

Keywords: Human T cells, Piezo1, Mechanosensing, Migration, Chemokine, Chemotaxis, Focal adhesion kinase, LFA-1, F-actin, Confocal Microscopy, Interference Reflection Microscopy

ABSTRACT

T cells are crucial for efficient antigen-specific immune responses and thus their migration within the body, to inflamed tissues from circulating blood or to secondary lymphoid organs, play a very critical role. T cell extravasation in inflamed tissues depends on chemotactic cues and interaction between endothelial adhesion molecules and cellular integrins. A migrating T cell is expected to sense diverse external and membrane-intrinsic mechano-physical cues, but molecular mechanisms of such mechanosensing in cell migration are not established. We explored if the professional mechanosensor Piezo1 play any role during integrin-dependent chemotaxis of human T cells. We found that deficiency of Piezo1 in human T cells interfered with integrin-dependent cellular motility. Piezo1 recruitment at the leading edge of moving T cells follows focal adhesion formation and local increase in membrane tension on chemokine receptor activation. Piezo1 activation constitutes a membrane-intrinsic component of the 'outside-in' signaling in human T cells, migrating in response to chemokines, that mediates integrin recruitment to the leading edge.

INTRODUCTION

In the steady-state as well as during an ongoing immune response migration of immune cells ensures optimal tissue antigen sampling, immunocellular interactions as well as effector functions (Shechter et al., 2013; Krummel et al., 2016). Among the adaptive immune cells T cells are key ones to orchestrate an efficient antigen-specific immune response and their migration to an inflamed tissue from circulating blood as well as into the secondary lymphoid organs thus plays a critical role (Woodland et al., 2009; Masopust et al., 2013). T cell migration in the body, e.g.; during extravasation in inflamed tissues, is dependent on chemotactic cues, interaction between endothelial adhesion molecules and T cell integrins, T cell integrin activation and an intricate acto-myosin dynamics (Fowell et al., 2021). The mechanical force generation is critical to propel the cells forward, achieved through a retrograde flow of actin and its interaction with myosin (Dupré et al., 2015; Nordenfelt et al., 2017; Moreau et al., 2018; Shannon et al., 2019). A role of mechanosensing of the substrate and increase in cellular membrane tension is also intuitively apparent in a migrating T cell, although mechanistic details are not explored to a great extent.

The ion-channel family of Piezo, the members being Piezo1 and Piezo2, has been recently discovered as an evolutionarily conserved family of mechanosensitive channels (Coste et al., 2010; Ranade et al., 2014a). Piezo proteins are professional mechanosensors that can sense increase in membrane tension mostly independent of other protein-protein interactions (Coste et al., 2012; Syeda et al., 2016). Mechanosensing by Piezo1 has been demonstrated to play critical role in diverse patho-physiologic contexts given its wide tissue expression, viz. development, cellular differentiation, red blood cell volume regulation, hemodynamic regulation, bone remodelling as well as cartilage function (Ranade et al., 2014a; Li et al., 2014; Lee et al., 2014; Cahalan et al., 2015; Zeng et al., 2018; Sun et al., 2019; Wang et al., 2020; Evans et al., 2020; Lee et al., 2021). Tissue expression and function of Piezo2 is rather restricted to the nervous system (Woo et al., 2014; Randa et al., 2014b). Previous studies by our group as well as others demonstrated wide expression of Piezo1 in the immunocellular compartment (Liu et al., 2018; Atcha et al., 2021; Geng et al., 2021; Jairaman et al., 2021; Jänttiet al., 2022). The role Piezo1-mechanosensing play in the regulation of the immune system hence has become an active area of research. On exploring the role of Piezo1 in human T cell activation we previously identified crucial role of this specialized mechanotransducer in optimal TCR triggering(Liu et al., 2018, Liu and Ganguly, 2019). A crucial role of Piezo1 in macrophage activation and effector function has also been demonstrated (Ma et. al., 2021; Atcha et al., 2021; Geng et al., 2021; He et al., 2022). The immunocellular expression of Piezo1 thus makes it a strong candidate for mechanosensing at the plasma membrane to regulate motility of immune cells.

A role of Piezo1 in cellular migration has been explored in different contexts, viz. cancer cells, fibroblasts, mesenchymal stem cells, keratinocytes, oligodendrocytes and macrophages, which show differential involvement of Piezo1 depending on contexts (Hung et al., 2016; Chubinskiy Nadezhdin et al., 2019; Mousawi et al.; 2020, Wang et al., 2021; Gao et al., 2021; Holt et al., 2021; He Y et al., 2022; Velasco-Estevez et al., 2022). The previous studies point to the possibility of a role of Piezo1 in confinement sensing and integrin activation in moving cells, while it deters integrin-independent cell motility, usually referred to as amoeboid movement (McHugh et al., 2010; Hung et al., 2016).

Here we aimed at exploring if Piezo1 mechanosensing plays any role during integrin-dependent chemotactic migration of human T cell migration, a patho-physiologically critical event in an ongoing immune response as well as in the steady-state. We found that deficiency of Piezo1 expression in human CD4 T cells as well as Jurkat T cells interfered with efficient integrin-dependent cellular motility in response to a chemotactic cue. We also found that Piezo1 activation constitutes a hitherto unknown membrane-intrinsic component of the 'outside-in' signaling in human T cells in response to chemokine receptor activation, that follows activation of focal adhesion kinase leading to local increase in membrane tension and mediates local recruitment of integrin molecules at the leading edge of the moving human T cells.

RESULTS

Piezo1 deficiency abrogates integrin-dependent chemotactic motility in human T cells

To explore the effect of deficiency of Piezo1 on human T cell migration, if any, first we assessed both integrin-independent and integrin-dependent non-directional motility of primary human $CD4^+$ T cells. Cells were nucleofected with either control or Piezo1-targeting siRNA (Supplemental figure 1A), with addition of the recombinant human chemokine CCL19 to the medium. For integrin-independent motility the cells were seeded on plastic culture plates, while to assess integrin-dependent movement the T cells were seeded on culture plates coated with recombinant human adhesion molecule, ICAM-1. As expected from previous data with murine keratinocyte migration in the context of in vitro scratch-wound healing (Holt et al., 2021), reduction in Piezo1 expression led to higher motility in human $CD4^+$ T cells too, in response to chemokine activation but seeded on bare plastic, in terms of mean squared displacement (MSD) (Supplemental figure 1B, C).

Interestingly, in case of integrin-dependent motility on ICAM-1-coated plates (referred to as ICAM-1 bed), which is physiologically more relevant in T cell biology, we found that siRNA-mediated reduction in Piezo1 expression abrogated optimal T cell motility in the presence of chemokine, in

terms of their movement over time, represented as mean square displacement or MSD (Figure. 1A). Comparison of cell trajectories (Figure 1B), total contour distance (d) traversed (Figure 1C) and the motility coefficient (Figure 1D, described in the methods), demonstrated inability of Piezo1-deficient $CD4^+$ T cells to move optimally on ICAM-1 bed. This intrigued us to explore the role of Piezo1 in integrin-dependent migration of human T cells in greater detail.

To assess whether these mechanosensors are also needed for directional motility of human T cells, we allowed control or Piezo1-trageting siRNA-transfected primary human $CD4^+$ T lymphocytes,to move across a gradient of human CCL19 in an ICAM-1-coated Millicell® μ-Migration chamber. The Piezo1-deficient $CD4^+$ T cells showed a dramatic reduction in the directional motility as well, as shown in terms of mean squared displacement (MSD) and total contour distance (d) traversed in Figure 1E and 1G. The dysregulation of directional motility of the Piezo1-deficient T cells was also apparent from their movement trajectories (Figure 1F), as well as directionality of movement, measured as the chemotactic index (Figure 1H, measured as described in the methods). The trailing tracks of the motile T cells as they move following the chemokine gradient in a representative microscopy field also reveal the migration inefficiency of the Piezo1-deficient cellsfor directional movement (Figure 1I, Supplemental videos 1,2).

Role of Piezo1 in human T cell chemotaxis was further confirmed in a three-dimensional transwell migration assay. Piezo1-deficient primary human $CD4^+$ T lymphocytes and Jurkat T cells both showed significant reduction in transwell migration in response to gradient of CCL19 and SDF1α, respectively (Figure 1J, K). Recombinant human SDF1α was used for Jurkat T cells as they were found to be more motile in response to this chemokine, compared to CCL19 (data not shown).

Redistribution of Piezo1 toward the leading edge of migrating T cells in response to chemotactic cue

Cell polarity, along the direction of the movement, is a crucial aspect of directional cell motility in response to chemokines. To understand the role of Piezo1 in T cell motility we wanted to understand if Piezo1 distribution in the cell changes in response to chemokine receptor activation. We seeded primary human $CD4^+$ T cells ICAM-1 bed and 30 min after addition of the chemokine CCL19, fixed the motile T cells and stained for Piezo1. This showed a striking polarity of Piezo1 distribution in the cells that experienced chemokine receptor activation, compared to untreated cells (Figure 2A,B; Supplemental video 3).

Next, to follow the dynamics of Piezo1 redistribution in a moving T cell we used Jurkat T cells, expressing Piezo1-mCherry, similarly seeded on ICAM-1-coated plate and added the chemokine SDF1α.As expected, this showed strikingly polar distribution of Piezo1 towards the leading edge within the lamellipodial structure of the Jurkat T cells, moving in response to SDF1α, as compared to cells not treated with the chemokine (Figure 2C). In Figure 2D, particle image velocimetry (PIV) analysis of a single representative Jurkat cell has been shown to display the dynamically polarized Piezo1 fluorescence upon SDF1α treatment with time, as opposed to rather uniformly distributed Piezo1 signals in a representative untreated cell. The continuous redistribution of Piezo1 within the motile T cells towards the leading edge can also be appreciated in the representative moving image provided (Supplemental video 4).

Piezo1 redistribution in migrating T cells follow increased membrane tension in the leading edge

Piezo1 is a professional mechanosensor ion channel, which senses increase in plasma membrane tension and responds by driving calcium influx into the cells (Liu et al., 2018; Liu and Ganguly, 2019; Xiao et al., 2020). As T cells migrate on substrate by extending membrane processes it is intuitive to hypothesize that a component of mechanosensing is incorporated in the mechanism of cellular movement. The data above, on a critical role of Piezo1 in migrating human T cells, also led us to hypothesize that Piezo1 mechanosensors may play a role in sensing mechanical cues in a moving T cell. So, first we aimed at confirming that there is polarized increase in tension in the leading edge plasma membrane of human T cells moving in response to a chemotactic cue.

Cellular membrane tension can be measured by various techniques. However, most of the usual techniques, viz. atomic force microscopy or tension measurement using optical tweezers, are invasive and interfere with the membrane dynamics, as well as are difficult to employ on a movingcells. To follow the membrane tension dynamics in Jurkat T cells, moving in response to the chemokine SDF1α, we utilized the non-invasive technique of interference reflection microscopy or IRM (Barr et al., 2009; Chakraborty et al., 2022). In IRM technique, steady-state local fluctuations in the plasma membrane is imaged in cells adhered to a glass coverslip. The interference patterns generated due to continuously changing local distance between the coverslip and the plasma membrane are computed to derive the magnitude of local tension in the membrane – lower temporal fluctuations represent an increase in membrane tension (Figure 3A).

We seeded Piezo1-GFP-expressing Jurkat T cells on recombinant human fibronectin-coated coverslips and performed sequential fluorescence and IRM imaging. After the cells were imaged by

IRM as the baseline, the chemokine SDF1α was added. Then the cells were subjected to sequential fluorescence and IRM imaging, followed till 31 min at around 2-3 min interval. This experiment revealed that chemokine administration to Jurkat T cells led to a decrease in temporal fluctuations and an increase in membrane tension when computed for the whole cellular contour (Figure 3B). The increase in membrane tension was registered within few minutes after chemokine addition and gradually declined over the 31 minutes of imaging (Figure 3C). Not just the overall tension, but distribution of tension and fluctuation-amplitude in cells was also affected by the action of chemokine (Supplemental figure 2A).

Moreover, the tension maps showed that the lamellipodial structures towards the leading edges of the cells had higher tension magnitudes (Figure 3D, Supplemental figure 2B). These high-tension edges are usually further emphasized at later time-points. The change in tension is accompanied by increase in the membrane's degree of confinement and the effective viscosity experienced (Supplemental figure 2C), which also show similar temporal pattern (Supplemental figure 2D).

Finally, we explored if local membrane tension increase was linked to Piezo1 redistribution in the chemokine-experienced T cells, by correlating the fluorescence images (showing Piezo1-GFP distribution) and the IRM tension maps. Of note here, during acquisition, there is typically a time delay of 1 minute between measurement of tension and Piezo1-GFP fluorescence. As expected, average tension peaked within the first few minutes of chemokine addition, followed by partial decline (Figure 3E) as seen for the whole cell. Pixel count of Piezo1-GFP intensity showed a similar pattern, albeit, at a delayed time, following the tension kinetics. In order to account for the delayed kinetics of tension magnitude and Piezo1-GFP pixel count, we performed a correlation between normalised Piezo1 pixel intensity at a particular time-frame, with normalised tension magnitude at the preceding time frame. We observed significant positive correlation between the two parameters (Figure 3F). The redistribution of the Piezo1 mechanosensors closely followed the dynamic higher tension regions in the cells, thus following membrane tension redistribution spatially (Figure 3F,G). Thus, IRM-coupled fluorescence microscopy revealed an increase in local membrane tension in the leading edge of the moving T cells in response to chemokine receptor activation that was associated with Piezo1 redistribution to the leading edges of the cells.

Focal adhesion following chemokine receptor activation does not depend on Piezo1

Focal adhesion formation is a critical step in cellular migration and activated (phosphorylated focal adhesion kinases link extracellular physical cues to the cytoskeletal actomyosin scaffold (Mitra et al.,

2005,Katoh et al., 2020). Chemokine signaling induces phosphorylation of focal adhesion kinase (FAK) and membrane recruitment of the FAK complex forming focal adhesions with the extracellular substrate. FAK recruits adapter proteins like paxillin to anchor with the local sub-membrane cytoskeleton made by de novo F-actin polymerization. Membrane-recruited FAK complexes anchored to cytoskeleton increases local membrane tension as well as recruit integrins to the membrane (Yamashiro et al., 2014; Dupré et al., 2015; Martino et al., 2018). This so-called 'outside-in' signaling, whereby membrane recruitment of integrins (e.g.; LFA1 in T cells) is initiated, is followed by integrin signaling ('inside-out' signaling) driven primarily by phosphoinositide 3-kinase (PI3K)-driven phosphorylation of Akt and downstream activation of Rho GTPases which in turn drive extensive F-actin polymerization (Sánchez-Martín et al., 2004; Roy et al., 2020). Retrograde flow of the F-actin to the rear end of the moving cells, through myosin-based contractions, generates the propelling force for cells to move forward following the chemokine gradient (Dupré et al., 2015; Nordenfelt et al., 2017).

Finding a critical role of Piezo1 in human T cell migration and a membrane tension-dependent redistribution of Piezo1 to the leading edge of the moving cells led us explore if FAK recruitment to the leading edge in response to chemokine receptor activation was dependent on Piezo1. On treating human $CD4^+$ T cells (seeded on ICAM-1 coated plates) with CCL19, we found striking polarity of phosphorylated FAK (pFAK), as expected (Figure 4A, B; Supplemental video 5). Upon performing the same experiment with control or Piezo1-targeting siRNA-transfected human $CD4^+$ T cells, Piezo1-deficiency was not found to affect pFAK polarity on chemokine addition (Figure 4C, D). Similarly, chemokine treatment showed prominent polarity of paxillin (Figure 4E, F), which again was not affected by Piezo1-defieciency in the siRNA-treated human $CD4^+$ T cells (Figure 4G, H). Thus, focal adhesion formation following chemokine receptor activation was not dependent on Piezo1.

On the other hand, FAK activation recruits adapters like paxillin and vinculin connecting the cortical cytoskeleton to the membrane and the extracellular matrix, thereby increasing local membrane tension (Mitra et al., 2005). To explore whether FAK-activation-driven increase in membrane tension trigger Piezo1 recruitment in the leading edge of migrating T cells, we inhibited FAK activation using an inhibitor on T cells treated with chemokine on ICAM1 bed. Inhibition of FAK activation completely abrogated Piezo1 redistribution to the leading edge, hence the polarity (Figure 4I, J). This indicated that mechanistically, FAK activation event precedes Piezo1 redistribution to the leading edge of the migrating human $CD4^+$ T cells.

Membrane recruitment of LFA1 on chemokine receptor activation disrupts with Piezo1 deficiency

Next, we wanted to explore if integrins recruitment to the leading edge, the critical step in cell migration, downstream of FAK activation and local F-actin polymerization, is affected by Piezo1 deficiency in the migrating T cells. Human $CD4^+$ T cell culture seeded on ICAM-1-coated plates was added with CCL19 followed by fixing of the motile cells and staining for LFA1 and Piezo1. As expected,chemokine receptor activation led to LFA1 recruitment to the leading edge (Figure 5A, B). Moreover, Piezo1 and LFA1 exhibited significant colocalization on addition of chemokine (Figure 5A, C; Supplemental video 6).

Then we followed this up with experiments wherein Piezo1 was downregulated in the human T cells using siRNA. Piezo1 deficiency significantly disrupted the cellular polarity and leadingedgerecruitment of LFA1 (Figure 5D, E; Supplemental videos 7, 8). Thus, role of Piezo1 in chemotactic migration of T cells was downstream of FAK assembly in response to chemokine receptor signaling, but preceded integrins recruitment. These data together point to a mechanism whereby local increase in membrane tension leading from FAK activation and assembly drives Piezo1 activation, which in turn is linked to LFA1 recruitment to the focal adhesions.

To further confirm this critical role of Piezo1 on LFA1 recruitment, we looked at the major signaling event downstream of LFA1 recruitment to the leading edge, i.e., phosphorylation of Akt downstreamof PI3K activation, which in turn is triggered upon integrin activation. On treatment with CCL19,human $CD4^+$ T cells moving on ICAM-1-coated plates did show a prominent leading-edge polarity ofnon-phosphorylated and phosphorylated Akt (pAkt) (Figure 5F control panel, Figure 5H). But inPiezo1-deficient cells the polarity of pAkt is abrogated, not affecting the polarity ofnon-phosphorylated AKT (Figure 5F, G; Supplemental videos 9, 10), substantiating the cellular signaling defect due to non-recruitment of LFA1 to the leading edge membrane.

Piezo1 deficiency disrupts F-actin retrograde flow in T cells despite chemokine receptor activation

Piezo1-mediated sensing of membrane tension drives calcium ion influx, which in turn has been shown to activate calpain and F-actin polymerization (Liu et al., 2018; Liu and Ganguly, 2019). LFA1 recruitment is driven by local actin scaffold formation following FAK assembly, which as our data indicates is perhaps contributed by consolidation local actin scaffold downstream of Piezo1 activation. To confirm this, we treated the human T cells with a calpain inhibitor (PD150606) before addition of chemokine to the cells, and looked at LFA1 polarity in the cells 30 min after chemokine addition. PD150606 did inhibit chemokine receptor activation induced LFA1 recruitment to the leading edge of the T cells (Figure 6A, B). As expected, the upstream event of pFAK polarity was not

affected by the calpain inhibitor PD150606 in the T cells experiencing chemokine receptor activation (Supplemental figure 3A, B).

While F-actin polymerization downstream of FAK is required for LFA1 recruitment, LFA1 in turn drives a more robust F-actin polymerization at the leading edge, through Akt phosphorylation and subsequent Rho GTPase activation. F-actin at the leading edge undergoes retrograde flow due to myosin-based contractility, thereby enabling cells to move forward. Thus, both at the leading edge lamellipodia and the rear edge F-actin redistribution can be documented in a motile cell. In our experiment with the human T cells moving in response to CCL19, focal co-localization of LFA1 with F-actin was seen in the leading edge, along with a denser actin-rich protrusion in the rear edge, which constitute the so-called uropod in moving cells (Figure 6A). In presence of the calpain inhibitor, this uniquely bipolar distribution of actin also disappeared (Figure 6A, C). This data suggested that LFA1 recruitment may depend on local F-actin polarization downstream of Piezo1 activation. On the other hand, failure of LFA1 recruitment and activation halts further F-actin polarization feeding the retrograde flow of actin during migration. When both Piezo1 and F-actin was stained 30 min after chemokine addition to primary T cells, the dichotomy of Piezo1 (dense leading edge distribution) and F-actin (more dense at the rear end) distribution was clearly demonstrated (Figure 6D; Supplemental video 11). But, no F-actin polarity was seen on downregulating Piezo1 in the T cells (Figure 6E, F; Supplemental videos 12, 13).

LFA1 activation-induced polymerization of F-actin, here found to be dependent on Piezo1 recruitment to the leading edge, is subjected to dynamic retrograde flow, with F-actin accumulation at the rear end uropod. Thus, to confirm this model, live cell imaging was performed on Jurkat T cells, expressing Piezo1-mcherry and actin-GFP. These Jurkat T cells were allowed to migrate on ICAM-1-coated dishes in the presence or absence of SDF1α (Supplemental figure 3C). Polarity in terms of front and back distribution of the F-actin and Piezo1 fluorescence signals was determined for the moving cells (as described in the methods). Figure 6G & H shows data computed across 15 minutes of live imaging to register the trans-temporal dynamics. Chemokine addition showed significant increase in Piezo1 polarity to the front end, as shown in the earlier experiments (Figure 6G, H; Supplemental figure 3D, left). But in case of F-actin a dynamic balance between leading edge and rear end was evident, as expected due to the retrograde flow of F-actin in migrating cells (Figure 6H, Supplemental figure 3D, right). Polar plots depicting angular distribution of Piezo1 mCherry and actin-GFP (over all time-points) in the presence or absence of SDF1α are shown in Supplemental figure 3E. Figure 6I, which is a representative frame of the live microscopy image acquisition, and the supplemental video 14 shows Piezo1-mCherry distribution predominantly at the leading edge and

actin-GFP eventually accumulating at the rear end in uropod-like cellular extensions in a migrating Jurkat T cell.

Thus, our data reveals a membrane-intrinsic event, involving a critical role of Piezo1 mechanosensors, within the outside-in signaling module in response to chemokine receptor activation in human T cells. The mechanistic model derived from our data is depicted in Figure 7. The Piezo1 mechanosensing links the focal adhesion assembly to integrins recruitment at the leading edge of the human T cells migrating in response to chemokine activation and thus play a critical role in chemotactic migration of human T cells.

DISCUSSION

The present study explored the role of membrane-intrinsic tension generation and the crucial role of sensing this physical cue in the context of human T cell migration in response to chemokine receptor activation. As described, response to chemotactic cue by T cells in terms of integrin-driven cellular migration is a critical event in an immune response as well as in the steady-state. While migrating, the cells experience intuitively obvious physical cues from the extracellular substrate along with differential membrane tension at the leading edge. We hypothesized that the professional mechanosensor protein Piezo1, which is expressed in human T cells, may play a role in sensing these physical cues to optimize the cell migration mechanism.

Interestingly, on comparing human T cells experiencing the chemokine signal on a bare plastic plate with those seeded on an ICAM1-bed revealed a differential migratory response in terms of the nature of involvement of the Piezo1 mechanosensors. Deficiency of Piezo1 enhanced integrin-independent motility of T cells but inhibited integrin-dependent migration. Previous experiments with different immune cells migrating on substrate without any cell adhesion molecules have also demonstrated similar deterrence of cell motility by Piezo1 (Huang et al., 2019; Chubinskiy-Nadezhdin et al., 2019; Holt et al., 2021). It was demonstrated in keratinocytes that in such movements, usually referred to as amoeboid movement, Piezo1 was recruited to the rear edge of the cells and presumably prevented the forward-propelling force generation in the cells in some as of yet unclear mechanism (Holt et al., 2021). As the integrin-dependent chemotactic migration of T cells on a substrate presenting cell adhesion molecules (viz. ICAM1) is a critically implicated in most patho-physiologic contexts, in the present study we focused on the potential role of Piezo1 mechanosensors in this specific context. Deficiency of Piezo1 expression abrogated the integrin-dependent motility of the human T cells (both primary human $CD4^+$ T cells as well as the Jurkat T

cells) in response to chemokine receptor activation, thus implicating a crucial role of these mechanosensor ion channels in this mode of cellular migration in human T cells.

Notably, a previous study in vivo in mice, using genetic deletion of Piezo1 in T cells, reported no significant effect on tissue recruitment of T cells (Jairaman et al., 2021). Although a functional redundancy in the role of Piezo1-mediated mechanosensing in mouse T cells warrants exclusion, especially in case of gene deletion in developing T cells, given the considerable expression of Piezo2 as well in mouse T cells (Ganguly, 2021). On the other hand, a role of Piezo1 activation in fibroblastic reticular cells in Peyer's patches has been shown to regulate lymphocyte migration through tissue conduits (Chang et al., 2019). The different tissue distribution of Piezo1 and Piezo2 expression in humans warranted exploring the role of Piezo1 in migrating human T cells, as in humans Piezo2 is hardly expressed in the hematopoietic cells.

We demonstrated that in response to chemokines there is a dynamic change in the membrane tension at the leading edge of the human T cells moving on an ICAM1-bed. This could be achieved through the uniquely non-invasive interference reflection microscopy, which measures magnitude of spontaneous membrane fluctuations and computes local membrane tension, based on the principle that these fluctuations are reduced in magnitude as the cell membrane experiences greater tension. Moreover, the localized increase in membrane tension was closely followed by dynamic recruitment of the professional mechanosensor Piezo1 locally. Chemokine receptor activation leads to focal adhesion formation at the leading edge of the migrating T cells (Mitra et al., 2005; Katoh et al., 2020). Our experiments revealed that Piezo1 recruitment at the leading edge of the cells followed focal adhesion kinase activation, as inhibition of focal adhesion kinase abrogated this event. Focal adhesions do increase local membrane tension as they connect the extracellular environment with the cortical cytoskeleton of the cell (Mitra et al., 2005). Piezo1 recruitment locally seems to be a response to this membrane tension increase at focal adhesions.

The so-called outside-in signaling downstream of focal adhesion formation recruits integrins to the leading edge of the moving T cells (Yamashiro et al., 2014; Dupré et al., 2015, Martino et al., 2018). We found that deficiency of Piezo1 abrogated this response, indicating that Piezo1 activation in response to local membrane tension is a component of this outside-in signaling. Piezo1 has been shown to drive Ca^{2+} influx into the T cells leading to calpain activation (Liu et al., 2018; Liu and Ganguly, 2019). As expected, calpain inhibition also interfered with leading edge recruitment of the integrin LFA-1. Plausibly calpain activation drives local F-actin polymerization at the leading edge facilitating LFA-1 recruitment and stability. This was also supported by loss of polarity of AKT phosphorylation with Piezo1 deficiency, which is known to be the major downstream signaling

module that succeeds LFA-1 recruitment and activation (Roy et al., 2018, Roy et al., 2020). These dysregulations in turn abrogates the retrograde flow of actin in the moving cell that is essential for forward propulsion of the cell body (Sánchez-Martín et al., 2004; Dupré et al., 2015; Nordenfelt et al., 2017; Roy et al., 2018).

Of note here, a role of Piezo1, present in the membrane of endoplasmic reticulum, in driving R-RAS-driven activation of integrins, which was again dependent on calpain activation, was reported even before the mechanosensing function of Piezo1 was established (McHugh et al., 2010). Thus, Piezo1 seems to play crucial role in integrin activation in response to both extracellular and intracellular cues.

Thus, the present study reports a hitherto unexplored role of the professional mechanosensor Piezo1 in integrin dependent chemotactic movement of human T cells. In the cascade of leading edge events in a moving human T cell, following chemokine receptor activation and eventually leading to the retrograde flow of actin, focal adhesion formation precedes Piezo1 activation, while LFA-1 recruitment is dependent on Piezo1 function.

MATERIALS AND METHODS

Human $CD4^+$ T cell isolation and transfection.

Human $CD4^+$ T lymphocytes were isolated from peripheral blood through magnetic immunoselection. Cells were transfected with either EGFP control or Piezo1-specific siRNAs using Lonza 4D nucleofector, as per the manufacturer's protocol. Briefly, cells were nucleofected in 100µl of supplemented P3 primary buffer containing 75ng of respective siRNAs. Nucleofection was performed using EO-115 pulse in Lonza 4D nucleofector. Nucleofected cells were incubated at 37°C. 5% CO_2 in RPMI media containing 10% FBS for 3 days before experiments were conducted.

2-dimensional cell tracking.

96-well plates were coated with 4µg/ml of recombinant human ICAM-1 overnight at 4°C. Wells were washed with 1X PBS. Control or Piezo1-specific siRNA-nucleofected $CD4^+$ T lymphocytes were stained with cell-trace dyes to allow easy detection during tracking. Stained cells were added to the wells and allowed to settle for 15 mins at 37°C. Since 2D tracking was performed at room temperature, 0.5µg/ml of recombinant human CCL19 was added to the cells at room temperature and incubated for 10 minutes before acquisition. Images were acquired at regular intervals at room temperature using EVOS FL microscope at 20X magnification for a total duration of 10-15 minutes. $CD4^+$ T

lymphocytes were RPMI without phenol red supplemented with 10% FBS and 25mM HEPES during the duration of imaging.

2D chemotaxis

Millicell®µ-Migration chambers were coated with 4µg/ml of recombinant human ICAM-1 as before. siRNA-nucleofected $CD4^+$ T lymphocytes, stained with cell trace dyes, were added to the lower section of the migration chamber and allowed to adhere for 15 minutes at 37°C. Recombinant human CCL19 was added at a final concentration of 0.5µg/ml to the upper section of the migration chamber. The chamber was incubated at room temperature for 10 minutes before acquisition. Imaging was performed at room temperature at regular intervals for a total duration of 10-15 minutes.

2D cell tracking analysis

Time-based image stacks obtained were analysed using the Particle Tracker 2D/3D plugin of the FIJI Mosaic Suite. Briefly, images were corrected for any shift in alignment during acquisition, using the StackReg plugin. Corrected images were the thresholded to create a 0-255 binary mask which were then used for tracking using the Particle Tracker 2D/3D plugin. Tracking provided frame-wise X-Y co-ordinates of cells which were subsequently used to derive the following parameters to measure motility:

a. Mean-squared displacement

MSD (n) = $\sum_{i=0}^{i=n}(x_n - x_0)^2 + (y_n - y_0)^2$ where,

i = 0 is the first frame,

i = n is the nth frame.

Totalcontour distance (Euclidean distance), (d) travelled

$\sum_{i=0}^{i=n}\sqrt{(x_{n+1} - x_n)^2 + (y_{n+1} - y_n)^2}$where,

'n' and 'n + 1' are subsequent frames.

Motility coefficient was calculated from the MSD versus time plot using the formula $\frac{\mu^2}{4t}$, where, µ is the slope of the graph and t is the total time interval.

Chemotactic Index (CI) was used to assess the degree of directional migration. It was calculated as the ratio between the distance travelled at the last frame with respect to its starting point (√MSDnth frame) and total distance travelled between each successive frame till the last time-point (total euclidean distance). A perfectly directional migration will cause these two parameters to be equal and hence, the ratio between them to be equal to 1.

Chemotactic Index (CI) = $\frac{\sqrt{MSD(n)}}{d}$

Tranwell chemotaxis assay

5µm transwell inserts were coated with 4µg/ml of recombinant human ICAM-1. Equal number of primary human $CD4^+$ T cells and Jurkat cells nucleofected with control or Piezo1-specific siRNA were added to the ICAM-1-coated inserts. Cells wereallowed to migrate in response to recombinant human CCL19 (0.5µg/ml) or SDF1α (0.1µg/ml) in the lower chamber wells for 5 hours and 1.5 hours, respectively, at 37°C, 5% CO_2. Migration was halted by placing the setup on ice. Percent migration was calculated by counting the number of cells in the lower chamber and dividing it by total number of cells that was seeded.

Overexpression of mCherry/GFP-tagged Piezo1 and Actin-GFP in Jurkat cells.

GFP and mCherry-tagged Piezo1 constructs were kindly provided byDr. Charles Cox at Victor Chang Cardiac Research Laboratory, Darlinghurst, Australia. Approximately 2 million Jurkat cells were nucleofected with 2-3µg of fluorescent Piezo1 construct in 100µl of supplemented SE cell line buffer. Cells were pulsed using CL-120 program in Lonza 4D nucleofector. Cells were cultured in antibiotics-deficient RPMI supplemented with 20% FBS for 36 hours.Overexpression was confirmed using flow cytometry.

Interference Reflection Microscopy and Analysis

Jurkat cells were nucleofected with 2-3µg/ml of Piezo1-GFP construct. Overexpression was confirmed using flow cytometry. Transfected cells were seeded on recombinant human fibronectin glass-based dishes. Cells were allowed to completely adhere for 1 hour to allow IRM imaging.

An inverted microscope (Nikon, Japan) with 60x 1.2 NA water-immersion objective, Hg arc lamp and necessary interference filter (546 ± 12 nm) were used for the interference reflection microscopy (Limozin and Sengupta, 2009; Biswas et al., 2017) and images were captured at 19.91 frames per second using a EMCCD camera (Evolve 512 Delta; Photometrics, Trenton, NJ). Cells that were significantly adhered to the glass bottom were used for imaging. Regions used for analysis were

stringently chosen to avoid parts farther than ~ 100 nm from the coverslip – also called the first branch region (FBR) and the size chosen was 4x4 pixels corresponding to ~ $(720\ nm)^2$. First, cells were imaged by IRM to take baseline reading following which chemokine (SDF1α) was added.Cells were followed till 30 min with ~ 2-3 min interval post-chemokine addition.

For stringent selection of subset of regions, extraction of parameters as well as for visualizing the amplitude of fluctuations, the methodology developed previously (Biswas et al., 2017, Biswas et al., 2019) was followed. 2048 frames corresponding to ~ 102 sec were captured and used for a single measurement of tension. The analysis involved calculation of standard deviation of temporal height fluctuations (SD_{time}) and estimating the power spectral density (PSD) by autoregressive technique (probability of covariance or pcov) where the order is chosen to match best with PSD obtained using fast fourier transform (MATLAB, Mathworks Inc., USA). For deriving mechanical parameters, the PSD is fitted with a Helfrich-based model –

$$PSD(f) = \frac{4\eta_{eff} A k_B T}{\pi} \int_{q_{min}}^{q_{max}} \frac{dq}{(4\eta_{eff}(2\pi f))^2 + \left[\kappa q^3 + \sigma q + \frac{\gamma}{q}\right]^2}$$

with four fitting parameters (Biswas et al., 2017)using fluctuation-tension (σ), effective viscosity (η_{eff}), level of confinement (γ) and the effective active temperature (*A*)). The bending rigidity (κ) was fixed at 15 k_BT. Membrane fluctuation-tension closely follows membrane frame tension for a large range of tension values (Shiba et al., 2016). Membrane fluctuation-tension closely follows membrane frame tension for a large range of tension values (Shiba et al., 2016). For brevity, membrane fluctuation-tension has been referred to as "tension" in the rest of the manuscript. Tension maps were created from PSDs calculated for every pixel which were subsequently fitted and parameters extracted for every pixel. For analysing correlation between fluorescence and tension, first the fluorescence distribution of cells was plotted. Regions of intermediate intensity (around the first peak of the distribution) of a fixed intensity range was filtered and the pixel count of the filtered area was plotted against the average tension in those pixels. Normalization was done by diving by the maximum value in the time series. Normalized pixel count, thus, reflects how area with high Piezo1-GFP at the membrane changes while avoiding a small area fraction with very high Piezo1-GFP which might arise from internal structures.To ensure significance of the observed differences, the statistical test undertaken was the Mann-Whitney U test.

Piezo1 and actin distribution in live cell imaging

Jurkat cells expressing mCherry-tagged Piezo1 were seeded on ICAM-1-coated dishes. 0.1µg/ml of recombinant human SDF1α was added to the cells for 15 minutes prior to imaging. Cell tracking was

performed in EVOS FL microscope using the PE-Texas red filter, at an interval of 1 frame per minute, at room temperature. Imaging was performed for a total duration of 15 minutes.

For Jurkat cells transfected with Piezo1-mcherry and actin-GFP, cells were treated similarly and acquired on Zeiss LSM confocal setup. Z-stack was obtained at 1µm per stack to capture the entire cell. Time-lapse was imaged at an interval of 30 second per frame for a total duration of 5 minutes. Confocal imaging was performed at 37°C.

For particle image velocimetry (PIV) analysis of Piezo1-mCherry-expressing Jurkat cells was performed using the Iterative PIV plugin of FIJI. Time-lapse image stacks were split and stacks of paired subsequent images were formed. Each of these stacks was then corrected for any shift in alignment using the StackReg plugin. Aligned stacks were then subjected to iterative FIJI PIV analysis using the conventional cross-correlation method to measure flow of fluorescent Piezo1 in chemokine-treated Jurkat cells. PIV post-processing was done with default parameters and PIV magnitude plots were obtained from the plugin.

Measurement of cell polarity during live-cell imaging.

A custom code was written in Fiji (ImageJ) to analyze the cell image time-lapse for the calculation Front/Back (F/B) ratio of actin and Piezo1 expression relative to the direction of cell migration. Briefly, intensity-based thresholding was performed on the actin images to create binary masks of the cells. Individual cell boundaries were identified in the time-lapse, which were stored in the form of polygon ROIs. The cell ROIs enabled the computation of each cell's trajectory and displacement vectors from the geometrical centroid at every frame of the time-lapse video. The computation of cell polarity involved fitting each cell's ROI to an ellipse and bisecting the ellipse perpendicular to the migration direction. The ratio of total intensities in the leading half and the trailing half of the ellipse was calculated for actin and piezo1 images to get the F/B ratio.

For polarity measurement of fixed confocal images, cell boundaries were similarly identified. Stored ROIs were then split into two halves perpendicular to the long axis of the cell. The polarity index was measured by calculating the difference of total intensities of two halves of the cell divided by the sum of their total intensities. A measurement of 1 shows complete skewing of fluorescent signals to one half of the cell, while a value of 0 shows uniform distribution of fluorescent signals in both cell halves Representative polarity analysis Piezo1 (fixed), Piezo1 mCherry (live), pFAK (fixed), paxillin (fixed), CD11a/LFA-1 (fixed) and actin (fixed) of untreated and CCL19-stimulated $CD4^+$ T lymphocytes (Supplemental figure 4A-F).

Generation of Piezo1 mCherry and Actin-GFP polar plots.

For analysis of angular/spatial distribution of Piezo1 mCherry and actin-GFP with respect to direction of cell movement, cell ROIs were applied to the actin and piezo1 channels individually, to find the intensity-weighted centre of mass (through all the time-points). Depending on the fluorescence intensity distribution, the intensity-weighted centre of mass is shifted away from the geometric centroid and towards the direction of a higher protein distribution. Thus, a vector connecting the centroid (geometric centre) to the centre of mass gives the direction of polarization of the protein of interest. The relative angle of the polarization vector against the cell displacement vector was calculated for each frame, and a polar histogram of the angles was plotted for actin-GFP and piezo1-mCherry.

Fixed immunostaining for confocal imaging

Untransfected human $CD4^+$ T lymphocytes were seeded on 12-mm, ICAM-1-coated glass coverslips at a density of about 0.2 million cells per coverslip. Cells were incubated at 37°C, 5% CO_2 for 1.5 hours. 0.5µg/ml of recombinant human CCL19 was added to each coverslip and incubated for 20-30 minutes at 37°C. Post-treatment, cells were fixed in 4% paraformaldehyde for 15 minutes at room temperature. Blocking was performed in 3% bovine serum albumin in 1X PBS containing 0.2% Triton X-100 for 50 minutes at room temperature. Primary rabbit anti-human Piezo1 (Proteintech) was added at a dilution of 1:100 (5µg/ml) and incubated at room temperature for 1 to 1.5 hours. Alexa 568-conjugated anti-rabbit IgG was added at a dilution of 1:350 (5.7µg/ml), and incubated for further 45-50 minutes. Nuclear staining was performed for 1 minute with Hoechst 33342 dye at a concentration of 1µg/ml in 1X PBS. All washes between steps were carried out in 1X PBS. Stained cells were then mounted on Vectashield® mounting media and sealed before confocal imaging.

For actin imaging, LifeAct-TagGFP2 protein was added at a concentration of 0.5µg/ml, and incubated for 45 minutes at room temperature before washing. For LFA-1 ($\alpha_L\beta2$) staining, mouse anti-human CD11a (α_L subunit) was added at a concentration of 5µg/ml, followed by addition of anti-mouse Alexa 594-conjugated IgG. For LFA-1 and Piezo1 co-staining, primary antibodies were added at above concentrations, with Alexa 568-conjugated anti-rabbit IgG (for Piezo1) and Alexa 488-conjuagted anti-mouse IgG (for CD11a/LFA-1).Mouse anti-human paxillin, clone 5H11, and rabbit/mouse anti-phosphorylated FAK (Tyr-397) were used to stain paxillin and pFAK, respectively. Paxillin and pFAK were stained to detect focal adhesions. These cells were treated with chemokine CCL19 for 10 minutes prior to fixation. While doing confocal microscopy, Z-stacks were captured at 0.5µmintervals. Confocal images are represented are maximum intensity projections of the Z-slices. 3Dprojectionfunction of Fiji wasused to create a 3D rendering of the Z-slices, using the brightest pointmethod of projection.

Calpain Inhibition

PD150606 (Merck, India), a non-competitive calpain 1 and 2 inhibitors, was used at a concentration of 100µM. Untransfected $CD4^+$ T lymphocytes were treated with PD150606 for 1 hour at 37°C prior to treatment of chemokine. Post -chemokine treatment cells were stained either with pFAK or paxillin as described.

Focal adhesion kinase Inhibition

FAK inhibitor 14 (1,2,4,5-Benzenetetraamine tetrahydrochloride) was used to selectively inhibit FAK activity. Inhibitor was added at a final concentration 10µM, 1 hour prior to treatment with recombinant CCL19. Post-treatment with CCL19, $CD4^+$ T lymphocytes were stained with Piezo1 for confocal imaging.

Statistics

All statistical significance was calculated using GraphPad Prism 8.0. Student t-test was used to calculate significance.

ACKNOWLEDGEMENTS

The study was funded by Council of Scientific and Industrial Research, India (Grant no. FBR MLP-140). D.G. is a recipient of Swarnajayanti Fellowship from Department of Science and Technology, Government of India. The authors express their gratitude for provision of the Piezo1 constructs by Dr. Charles Cox, Victor Chang Institute of Cardiac Research, Australia.

The authors declare no competing interests

C.S.C.L. designed, performed and analyzed most of the experiments, prepared the figures and took part in writing the manuscript; T.M., B.S. and C.S.C.L. performed the IRM experiments; T.M. and B.S. analyzed IRM data; C.S.C.L., P.B. and D.K.S. performed image analyses; Pu.B., M.A.H., B.P.S., J.S. and R.D. helped with cell culture and confocal microscopy experiments; D.G. conceptualized and supervised the study, acquired funding, designed experiments and wrote the manuscript with input from all authors.

REFERENCES

Atcha H., A.Jairaman, J.R.Holt, V.S.Meli, R.R.Nagalla, P.K.Veerasubramanian,K.T.Brumm, H.E.Lim, S.Othy, M.D.Cahalan, et al., 2021. Mechanically activated ion channel Piezo1 modulates macrophage polarization and stiffness sensing. Nat Commun. 12:3256. doi: 10.1038/s41467-021-23482-5.

Barr V.A., and S.C.Bunnell. 2009. Interference reflection microscopy. CurrProtoc Cell Biol. Chapter 4:Unit 4.23. doi: 10.1002/0471143030.cb0423s45.

Biswas A., A. Alex, and B. Sinha. 2017. Mapping Cell Membrane Fluctuations Reveals Their Active Regulation and Transient Heterogeneities. Biophys J.113:1768-1781. doi: 10.1016/j.bpj.2017.08.041.

Biswas A., P. Kashyap, S. Datta, T. Sengupta, and B. Sinha. Cholesterol Depletion by MβCD Enhances Cell Membrane Tension and Its Variations-Reducing Integrity. Biophys J. 2019 Apr 23;116:1456-1468.

Cahalan S.M., V. Lukacs, S.S. Ranade, S. Chien, M. Bandell, andA. Patapoutian. 2015. Piezo1 links mechanical forces to red blood cell volume. Elife. 4:e07370. doi: 10.7554/eLife.07370.

Chakraborty M., B. Mukherjee, N. Nalinakshan, A. Biswas, R.K. Nayak, andB. Sinha. 2022. Effect of heterogeneous substrate adhesivity of follower cells on speed and tension profile of leader cells in primary keratocyte collective cell migration. Biol Open.11:bio058893. doi: 10.1242/bio.058893.

Chang J.E., M.B. Buechler, E. Gressier, S.J. Turley, andM.C. Carroll. 2019.Mechanosensing by Peyer's patch stroma regulates lymphocyte migration and mucosal antibody responses. Nat Immunol. 11:1506-1516. doi: 10.1038/s41590-019-0505-z.

Chubinskiy-Nadezhdin VI., V.Y. Vasileva, I.O. Vassilieva, A.V. Sudarikova, E.A. Morachevskaya, and Y.A. Negulyaev. 2019. Agonist-induced Piezo1 activation suppresses migration of transformed fibroblasts. BiochemBiophys Res Commun. 514:173-179. doi: 10.1016/j.bbrc.2019.04.139.

Coste B., J. Mathur, M. Schmidt, T.J. Earley, S.S. Ranade, M.J. Petrus, A.E. Dubin, and A. Patapoutian. 2010. Piezo1 and Piezo2 are essential components of distinct mechanically activated cation channels. Science. 330:55-60. doi: 10.1126/science.1193270.

Coste B., B. Xiao, J.S. Santos, R. Syeda, J. Grandl, K.S. Spencer, S.E. Kim, M. Schmidt, J. Mathur, A.E. Dubin, et al. 2012. Piezo proteins are pore-forming subunits of mechanically activated channels. Nature. 483:176-81. doi: 10.1038/nature10812.

Dupré L., R. Houmadi, J. Tang C, and J. Rey-Barroso. T Lymphocyte Migration: An Action Movie Starring the Actin and Associated Actors. 2015. Front Immunol.6:586. doi: 10.3389/fimmu.2015.00586.

Evans E.L., O.V. Povstyan, D. De Vecchis, F. Macrae, L. Lichtenstein, T.S. Futers, G. Parsonage, N.E. Humphreys, A. Adamson, A.C. Kalli, et al. 2020. RBCs prevent rapid PIEZO1 inactivation and expose slow deactivation as a mechanism of dehydrated hereditary stomatocytosis. Blood. 136:140-144. doi: 10.1182/blood.2019004174.

Fowell D.J., and M. Kim. The spatio-temporal control of effector T cell migration. 2021. Nat Rev Immunol. 9:582-596. doi: 10.1038/s41577-021-00507-0.

Ganguly D. 2021. Can Piezo2 substitute Piezo1 function in the context of T cell-specific deletion in mice? Sci Adv, e-Letter published Sep 8, 2021, in response to Jairaman A et al.,

Gao L., Y. Ji, L. Wang, M. He, X. Yang, Y.Qiu, X. Sun, Z. Ji, G. Yang, J. Zhang, et al.2021. Suppression of Esophageal Squamous Cell Carcinoma Development by Mechanosensitive Protein Piezo1 Downregulation. ACS Omega. 6:10196-10206. doi: 10.1021/acsomega.1c00505.

Geng J., Y. Shi, J. Zhang, B. Yang, P. Wang, W. Yuan, H. Zhao, J. Li, F. Qin, L. Hong, et al. 2021. TLR4 signalling via Piezo1 engages and enhances the macrophage mediated host response during bacterial infection. Nat Commun.12:3519. doi: 10.1038/s41467-021-23683-y.

He Y., B. Deng, S. Liu, S. Luo, Y. Ning, X. Pan, R. Wan, Y. Chen, Z. Zhang, J. Jiang, et al. 2022. Myeloid Piezo1 Deletion Protects Renal Fibrosis by Restraining Macrophage Infiltration and Activation. Hypertension. 5:918-931. doi: 10.1161/HYPERTENSIONAHA.121.18750.

Holt J.R., W.Z. Zeng, E.L. Evans, S.H. Woo, S. Ma, H.Abuwarda, M. Loud, A.Patapoutian, M.M. Pathak. 2021. Spatiotemporal dynamics of PIEZO1 localization controls keratinocyte migration during wound healing. Elife. 10:e65415. doi: 10.7554/eLife.65415.

Huang Z., Z. Sun, X. Zhang, K.Niu, Y. Wang, J. Zheng, H. Li , and Y. Liu. 2019. Loss of stretch-activated channels, PIEZOs, accelerates non-small cell lung cancer progression and cell migration. Biosci Rep. 39:BSR20181679. doi: 10.1042/BSR20181679.

Hung W.C., J.R. Yang, C.L. Yankaskas, B.S. Wong, P.H. Wu, C. Pardo-Pastor, S.A. Serra, M.J. Chiang, Z. Gu, D. Wirtz, et al. 2016. Confinement Sensing and Signal Optimizaton via Piezo1/PKA and Myosin II Pathways. Cell Rep. 15:1430-1441. doi: 10.1016/j.celrep.2016.04.035.

Jairaman A., S. Othy, J.L. Dynes, A.V.Yeromin, A. Zavala, M.L. Greenberg, J.L. Nourse, J.R. Holt, S.M. Cahalan, F. Marangoni, et al. 2021. Piezo1 channels restrain regulatory T cells but are dispensable for effector CD4+ T cell responses. Sci Adv. 7:eabg5859. doi: 10.1126/sciadv.abg5859.

Jäntti H., V. Sitnikova, Y.Ishchenko, A.Shakirzyanova, L. Giudice, I.F. Ugidos, M. Gómez-Budia, N. Korvenlaita, S. Ohtonen, I. Belaya, et al. 2022. Microglial amyloid beta clearance is driven by PIEZO1 channels. J Neuroinflammation. 19:147. doi: 10.1186/s12974-022-02486-y.

Katoh K. 2020. FAK-Dependent Cell Motility and Cell Elongation. Cells. 9:192. doi: 10.3390/cells9010192.

Krummel M.F., F. Bartumeus, and A. Gérard. 2016. T cell migration, search strategies and mechanisms. Nat Rev Immunol. 16:193-201. doi: 10.1038/nri.2015.16.

Lee W., H.A. Leddy, Y. Chen, S.H. Lee, N.A. Zelenski, A.L. McNulty, J. Wu, K.N.Beicker, J. Coles, S. Zauscher, and J. Grandl, et al. 2014. Synergy between Piezo1 and Piezo2 channels confers high-strain mechanosensitivity to articular cartilage. Proc Natl Acad Sci U S A. 111:E5114-22. doi: 10.1073/pnas.1414298111.

Lee W., R.J. Nims, A. Savadipour, Q. Zhang, H.A. Leddy, F. Liu, A.L. McNulty, Y. Chen, F.Guilak, and W.B. Liedtke. 2021. Inflammatory signaling sensitizes Piezo1 mechanotransduction in articular chondrocytes as a pathogenic feed-forward mechanism in osteoarthritis. Proc Natl Acad Sci U S A. 118:e2001611118. doi: 10.1073/pnas.2001611118.

Li J., B. Hou, S.Tumova, K.Muraki, A. Bruns, M.J. Ludlow, A.Sedo, A.J. Hyman, L. McKeown, R.S. Young, et al. 2014. Piezo1 integration of vascular architecture with physiological force. Nature. 515:279-282. doi: 10.1038/nature13701.

Limozin L. and K. Sengupta. 2009. Quantitative reflection interference contrast microscopy (RICM) in soft matter and cell adhesion. Chemphyschem. 10:2752-68.

Liu C.S.C, and D. Ganguly. 2019. Mechanical Cues for T Cell Activation: Role of Piezo1 Mechanosensors. Crit Rev Immunol. 39:15-38. doi: 10.1615/CritRevImmunol.2019029595.

Liu C.S.C., D. Raychaudhuri, B. Paul, Y. Chakrabarty, A.R. Ghosh, O.Rahaman, A. Talukdar, andD. Ganguly. 2018. Cutting Edge: Piezo1 Mechanosensors Optimize Human T Cell Activation. J Immunol. 200:1255-1260. doi: 10.4049/jimmunol.1701118.

Ma S., A.E.Dubin, Y. Zhang, S.A.R. Mousavi, Y. Wang, A.M. Coombs, M. Loud, I.Andolfo, andA. Patapoutian. 2021. A role of PIEZO1 in iron metabolism in mice and humans. Cell. 184:969-982.e13. doi: 10.1016/j.cell.2021.01.024.

Martino F., A.R. Perestrelo, V. Vinarský, S. Pagliari, andG. Forte. 2018. Cellular Mechanotransduction: From Tension to Function. Front Physiol. 9:824. doi: 10.3389/fphys.2018.00824.

Masopust D., andJ.M. Schenkel. 2013. The integration of T cell migration, differentiation and function. Nat Rev Immunol. 13:309-20. doi: 10.1038/nri3442.

McHugh B.J., R. Buttery, Y. Lad, S. Banks, C. Haslett, and T. Sethi. 2010. Integrin activation by Fam38A uses a novel mechanism of R-Ras targeting to the endoplasmic reticulum. J Cell Sci.123:51-61. doi: 10.1242/jcs.056424.

Mitra S.K., D.A. Hanson, and D.D.Schlaepfer. 2005. Focal adhesion kinase: in command and control of cell motility. Nat Rev Mol Cell Biol. 6:56-68. doi: 10.1038/nrm1549.

Moreau H.D., M. Piel, R.Voituriez, and A.M. Lennon-Duménil. 2018. Integrating Physical and Molecular Insights on Immune Cell Migration. Trends Immunol. 39:632-643. doi: 10.1016/j.it.2018.04.007.

Mousawi F., H. Peng, J. Li, S. Ponnambalam, S. Roger, H. Zhao, X. Yang, and L.H. Jiang. 2020. Chemical activation of the Piezo1 channel drives mesenchymal stem cell migration via inducing ATP release and activation of P2 receptor purinergic signaling. Stem Cells. 38:410-421. doi: 10.1002/stem.3114.

Nordenfelt P., T.I. Moore, S.B. Mehta, J.M.Kalappurakkal, V. Swaminathan, N. Koga, T.J. Lambert, D. Baker, J.C. Waters, R.Oldenbourg, et al. 2017. Direction of actin flow dictates integrin LFA-1 orientation during leukocyte migration. Nat Commun. 8:2047. doi: 10.1038/s41467-017-01848-y.

Ranade S.S., Z.Qiu, S.H. Woo, S.S.Hur, S.E. Murthy, S.M.Cahalan, J. Xu, J. Mathur, M.Bandell, B. Coste, et al. 2014a. Piezo1, a mechanically activated ion channel, is required for vascular development in mice. Proc Natl Acad Sci U S A. 111:10347-52. doi: 10.1073/pnas.1409233111.

Ranade S.S., S.H. Woo, A.E. Dubin, R.A.Moshourab, C. Wetzel, M. Petrus, J. Mathur, V.Bégay, B. Coste, J.Mainquist, et al. 2014b. Piezo2 is the major transducer of mechanical forces for touch sensation in mice. Nature. 516:121-5. doi: 10.1038/nature13980.

Roy N.H., S.H.J. Kim, A.Buffone Jr, D. Blumenthal, B. Huang, S. Agarwal, P.L. Schwartzberg, D.A. Hammer, and J.K. Burkhardt. 2020. LFA-1 signals to promote actin polymerization and upstream migration in T cells. J Cell Sci. 133:jcs248328. doi: 10.1242/jcs.248328.

Roy N.H., J.L. MacKay, T.F. Robertson, D.A. Hammer, and J.K. Burkhardt. 2018.Crk adaptor proteins mediate actin-dependent T cell migration and mechanosensing induced by the integrin LFA-1. Sci Signal. 11:eaat3178. doi: 10.1126/scisignal.aat3178.

Sánchez-Martín L., N. Sánchez-Sánchez, M.D. Gutiérrez-López, A.I. Rojo, M. Vicente-Manzanares, M.J. Pérez-Alvarez, P. Sánchez-Mateos, X.R. Bustelo, A. Cuadrado, F. Sánchez-Madrid, et al. 2004. Signaling through the leukocyte integrin LFA-1 in T cells induces a transient activation of Rac-1 that is regulated by Vav and PI3K/Akt-1. J Biol Chem. 279:16194-205. doi: 10.1074/jbc.M400905200.

Shannon M.J., J. Pineau, J.Griffié, J. Aaron, T. Peel, D.J. Williamson, R. Zamoyska, A.P. Cope, G.H. Cornish, and D.M. Owen.2019. Differential nanoscale organisation of LFA-1 modulates T-cell migration. J Cell Sci. 133:jcs232991. doi: 10.1242/jcs.232991.

Shechter R., A. London, and M. Schwartz. 2013. Orchestrated leukocyte recruitment to immune-privileged sites: absolute barriers versus educational gates. Nat Rev Immunol. 13:206-18. doi: 10.1038/nri3391.

Shiba H., H. Noguchi, and J.B. Fournier. 2016. Monte Carlo study of the frame, fluctuation and internal tensions of fluctuating membranes with fixed area. Soft Matter. 12:2373-80. doi: 10.1039/c5sm01900a.

Sun W., S. Chi, Y. Li, S. Ling, Y. Tan, Y. Xu, F. Jiang, J. Li, C. Liu, G. Zhong, et al. 2019. The mechanosensitive Piezo1 channel is required for bone formation. Elife.8:e47454. doi: 10.7554/eLife.47454.

Syeda R., M.N. Florendo, C.D. Cox, J.M. Kefauver, J.S. Santos, B.Martinac, and A.Patapoutian. 2016. Piezo1 Channels Are Inherently Mechanosensitive. Cell Rep.17:1739-1746. doi: 10.1016/j.celrep.2016.10.033.

Velasco-Estevez M., N. Koch, I.Klejbor, F.Caratis, and A. Rutkowska. 2022. Mechanoreceptor Piezo1 Is Downregulated in Multiple Sclerosis Brain and Is Involved in the Maturation and Migration of Oligodendrocytes in vitro. Front Cell Neurosci. 16:914985. doi: 10.3389/fncel.2022.914985.

Wang L., X. You, S.Lotinun, L. Zhang, N. Wu, and W. Zou. 2020. Mechanical sensing protein PIEZO1 regulates bone homeostasis via osteoblast-osteoclast crosstalk. Nat Commun. 11:282. doi: 10.1038/s41467-019-14146-6.

Wang X., G. Cheng, Y. Miao, F.Qiu, L. Bai, Z. Gao, Y. Huang, L. Dong, X. Niu, X. Wang, et al. 2021. Piezo type mechanosensitive ion channel component 1 facilitates gastric cancer omentum metastasis. J Cell Mol Med. 25:2238-2253. doi: 10.1111/jcmm.16217.

Woo S.H., S. Ranade, A.D. Weyer, A.E. Dubin, Y. Baba, Z. Qiu, M. Petrus, T. Miyamoto, K. Reddy, E.A. Lumpkin, et al. 2014. Piezo2 is required for Merkel-cell mechanotransduction. Nature. 509:622-6. doi: 10.1038/nature13251.

Woodland D.L., and J.EKohlmeier. 2009. Migration, maintenance and recall of memory T cells in peripheral tissues. Nat Rev Immunol. 9:153-61. doi: 10.1038/nri2496.

Xiao B. 2020. Levering Mechanically Activated Piezo Channels for Potential Pharmacological Intervention. Annu Rev PharmacolToxicol. 60:195-218. doi: 10.1146/annurev-pharmtox-010919-023703.

Yamashiro S.,and N. Watanabe. 2014. A new link between the retrograde actin flow and focal adhesions. J Biochem. 156:239-48. doi: 10.1093/jb/mvu053.

Zeng W.Z., K.L. Marshall, S. Min, I.Daou, M.W.Chapleau, F.M. Abboud, S.D. Liberles, A., and Patapoutian. 2018. PIEZOs mediate neuronal sensing of blood pressure and the baroreceptor reflex. Science. 362:464-467. doi: 10.1126/science.aau6324.

FIGURE LEGENDS

Figure 1. Piezo1 deficiency abrogates integrin-dependent chemotactic motility in human T cells.

A. MSD versus time calculated for control (black) and Piezo1 (blue) siRNA-transfected human $CD4^+$ T lymphocytes, that were allowed to migrate in presence of recombinant CCL19 on ICAM1-coated dishes. N > 240 random cells each. **B.** Representative tracks of control (left) and Piezo1-knockdown (right) $CD4^+$ T lymphocytes. Comparisons of **C.** total distance traversed (d) (N > 240 random cells, each) and **D.** donor-wise motility coefficients of control (black) and Piezo1 (blue) siRNA-transfected human $CD4^+$ T lymphocytes, respectively. **E.** MSD versus time of siRNA-transfected $CD4^+$ T lymphocytes subjected to chemokine gradient in ICAM-1-coated, Millicell μ-migration chamber. N > 200 random cells, each. **F.** Representative tracks of control (left) and Piezo1-knockdown (right) $CD4^+$ T lymphocytes. **G.** Comparison of total distance traversed (d) by siRNA-transfected cells. N > 150 random cells, each. **H.** Chemotactic index depicting directionality of moving siRNA-transfected $CD4^+$ T lymphocytes in response to chemokine gradient in μ-migration chamber. N > 150 random cells, each. **I.** Representative field depicting migratory tracks of siRNA-transfected $CD4^+$ T lymphocytes in millicell μ-migration assay (10X magnification). **J & K.** 3D transwell migration assay of siRNA-transfected primary human $CD4^+$ T lymphocytes (J) and Jurkat T cells (K), respectively. Data representative of at least 3 independent experiments.

Figure 2. Redistribution of Piezo1 toward the leading edge of migrating T cells in response to chemotactic cue.

A. Representative confocal images of Piezo1 distribution in fixed untreated and CCL19-treated $CD4^+$ T lymphocytes. 63X oil magnification. **B.** Comparison between Piezo1 polarity index calculated for fixed, stained, human $CD4^+$ T lymphocytes with or without 0.5μg/ml CCL19 treatment for 20-30 minutes. n > 300 random cells, each.**C.** Piezo1 polarity index calculated for Jurkat cells, expressing mCherry-tagged Piezo1 during live-cell tracking in the presence of recombinant SDF1α. Each dot represents polarity index of each cell, averaged over all the time-frames. **D.** Representative time kinetics of particle image velocimetry (PIV)

analysis of Piezo1-mcherry transfected Jurkat cells, allowed to move on ICAM-coated dishes in the presence of recombinant SDF1α. Top panel: No chemokine. Bottom Panel: SDF1α.

Figure 3. Piezo1 redistribution in migrating T cells follow increased membrane tension in the leading edge.

A. Schematic illustration of interference reflection microscopy imaging setup. **B.** Probability distribution of amplitude of temporal fluctuations (SD_{time}, left) and tension (right) before and after addition of chemokines. **C.**Temporal trajectory of tension of cells before and after addition of chemokine with** indicating significant difference from control. **D.** Representative IRM images of Jurkat cells (top), corresponding tension maps (middle) and R^2 maps (bottom), before and after chemokine treatment. **E.** Correlation between normalized Piezo intensity, tension magnitudes with time. **F.** Scatter plot to show correlation between normalized pixel count of Piezo1 and normalized tension. Piezo1 intensity at specific time-points were correlated with tension magnitudes at the preceding timepoints. Normalization has been done such that the maximum value is set to 1 and others are accordingly scaled. **G.** Colour-coded Piezo1-GFP intensity map (left), epifluorescence image (middle), and tension map (right) of representativePiezo1-GFP expressing Jurkat cell, after 30 minutes of 0.1µg/ml of SDF1α treatment.

Figure 4. Focal adhesion following chemokine receptor activation does not depend on Piezo1.

A. Representative confocal images of human $CD4^+$ T lymphocytes, fixed and stained for phospho-FAK (pFAK) under untreated and CCL19-treated conditions. **B.** Increased polarity of pFAK upon chemokine stimulation of $CD4^+$ T lymphocytes as compared to unstimulated controls. n > 120 cells, each. **C.** Representative confocal images of pFAK distribution in control and Piezo1 siRNA-transfected $CD4^+$ T lymphocytes stimulated with chemokine. **D**. Comparison of pFAK polarity in CCL19-stimulated control and Piezo1-knockdown $CD4^+$ T lymphocytes. n > 450 random cells, each. **E.** Representative confocal images of paxillin distribution in untreated versus CCL19-stimulated $CD4^+$ T lymphocytes. **F.** Increased paxillin

polarity in response to CCL19 stimulation as compared to untreated $CD4^+$ T lymphocytes. Untreated n > 70, CCL19-treated n > 150. **G.** Representative confocal images of immunostained paxillin in chemokine-stimulated, control and Piezo1-knockdown $CD4^+$ T lymphocytes. **H**. Comparison of paxillin polarity in CCL19-stimulated control and Piezo1-knockdown $CD4^+$ T lymphocytes. n > 340 random cells, each. **I.** Representative confocal images of stained Piezo1 in $CD4^+$ T cells stimulated with CCL19 in the presence or absence of FAK inhibitor 14. **J.** Effect of FAK inhibition on Piezo1 polarity in $CD4^+$ T lymphocytes stimulated with recombinant CCL19 versus untreated cells. n > 600 random cells, each. Data represented from at least 3 independent experiments.

Figure 5. Membrane recruitment of LFA1 on chemokine receptor activation disrupts with Piezo1 deficiency.

A. Representative confocal images of fixed, immunostained Piezo1 and LFA1 in unstimulated and CCL19-stimulated $CD4^+$ T lymphocytes. **B.** Increased LFA1 polarity in response to recombinant CCL19 stimulation in $CD4^+$ T cells. n > 240 random cells, each. **C.**Manders' co-localisation analysis of Piezo1 and LFA1 in untreated and CCL19-treated $CD4^+$ T lymphocytes. **D.** Comparison of LFA1 polarity in chemokine-treated control and Piezo1 knockdown $CD4^+$ T lymphocytes. **E.** Representative confocal stained images of LFA1 polarity of CCL19-treated control and Piezo1-knockdown $CD4^+$ T lymphocytes. n > 490 random cells, each. **F.** Representative confocal images of phospho-Akt (pAkt) and Akt distribution upon chemokine treatment of control and Piezo1-knockdown cells. **G & H.** Quantitative analyses ofpAkt(G) and Akt (H) polarity in control and Piezo1-knockdown cells after CCL19-treatment. n > 580 random cells, each. All fixing and immunostaining were performed 30 mins after addition of 0.5µg/ml of recombinant CCL19. All stimulation was performed on recombinant ICAM1-coated coverslips. Data represented from at least 3 independent experiments.

Figure 6. Piezo1 deficiency disrupts F-actin retrograde flow in T cells despite chemokine receptor activation.

A. Representative confocal images of LFA1 and actin distribution in CCL19-stimulated $CD4^+$ T lymphocytes with or without inhibition of calpain. 100µM of PD15606 was added to the cells 1 hour prior to addition of chemokine. Quantitative comparisons of **B.** LFA1 and **C.** actin polarity upon chemokine stimulation, in the presence or absence of calpain pre-inhibition. n > 290 random cells, each. **D.** Representative fixed confocal images of actin and Piezo1 distribution in $CD4^+$ T lymphocytes after 30 mins of 0.5µg/ml recombinant CCL19 treatment. **E.** Representative fixed confocal images of actin distribution in chemokine-treated, control and Piezo1-knockdown $CD4^+$ T lymphocytes. **F.** Quantitative comparison of actin polarity in control and Piezo1-knockdown $CD4^+$ T lymphocytes cells after 30 mins of chemokine treatment. n > 300 random cells, each. **G & H.** Quantitative analyses of front/back polarity of Piezo1 and actin, calculated from 2D cell tracks, after live-cell imaging of Piezo1-mCherry and actin-GFP expressing Jurkat cells in untreated (G) and with SDF1α treatment (H). **I.** A snapshot of time-lapse imaging of Piezo1-mCherry and actin-GFP expressing Jurkat cell treated with 0.1µg/ml of SDF1α. Image is maximum Z-projection of the cell at 63X/1.40 magnification.

Figure 7. The mechanistic model depicting involvement of Piezo1 mechanosensing in leading edge events in a migrating T cell.

Chemokine receptor activation in human T cells lead to focal adhesion kinase activation and focal adhesion formation. Focal adhesions lead to localized increase in membrane tension at the leading edge plasma membrane which leads to Piezo1 recruitment and activation. Piezo1 activation leads to calpain activation which perhaps drives further cytoskeletal consolidation to recruit integrin LFA1. LFA1 recruitment and activation lead to phosphorylation of AKT and downstream signaling eventually driving the retrograde actin flow in migrating human T cells.

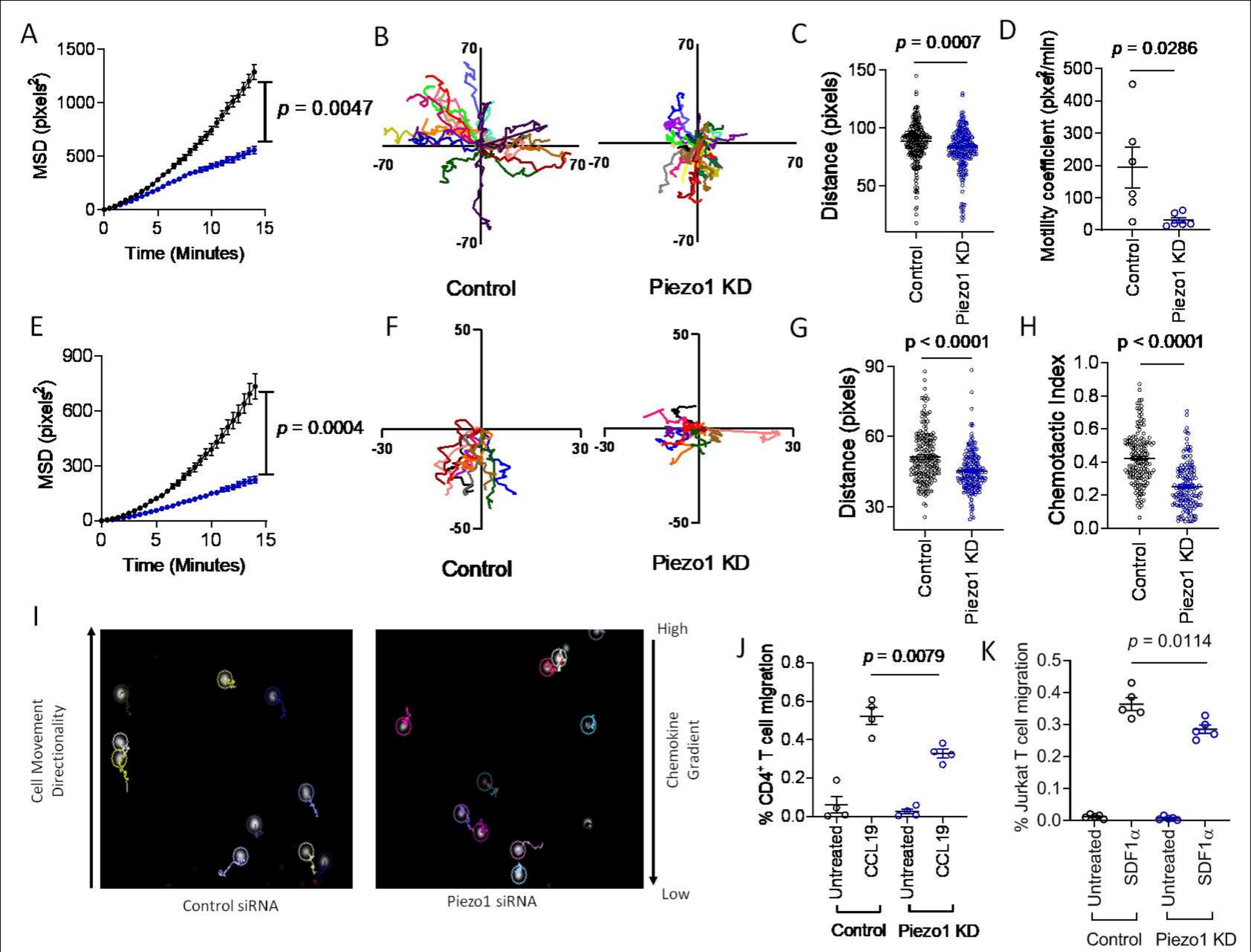
A
MSD (pixels²)
Time (Minutes)
p = 0.0047
B
Control
Piezo1 KD
C
Distance (pixels)
p = 0.0007
Control
Piezo1 KD
D
Motility coefficient (pixel²/min)
p = 0.0286
Control
Piezo1 KD
E
MSD (pixels²)
Time (Minutes)
p = 0.0004
F
Control
G
Piezo1 KD
Distance (pixels)
p < 0.0001
Control
Piezo1 KD
H
Chemotactic Index
p < 0.0001
Control
Piezo1 KD
I
Cell Movement Directionality
Control siRNA
Piezo1 siRNA
High
Chemokine Gradient
Low
J
% CD4⁺ T cell migration
p = 0.0079
Untreated
CCL19
Control
Piezo1 KD
K
% Jurkat T cell migration
p = 0.0114
Untreated
SDF1α
Control
Piezo1 KD

Figure 1

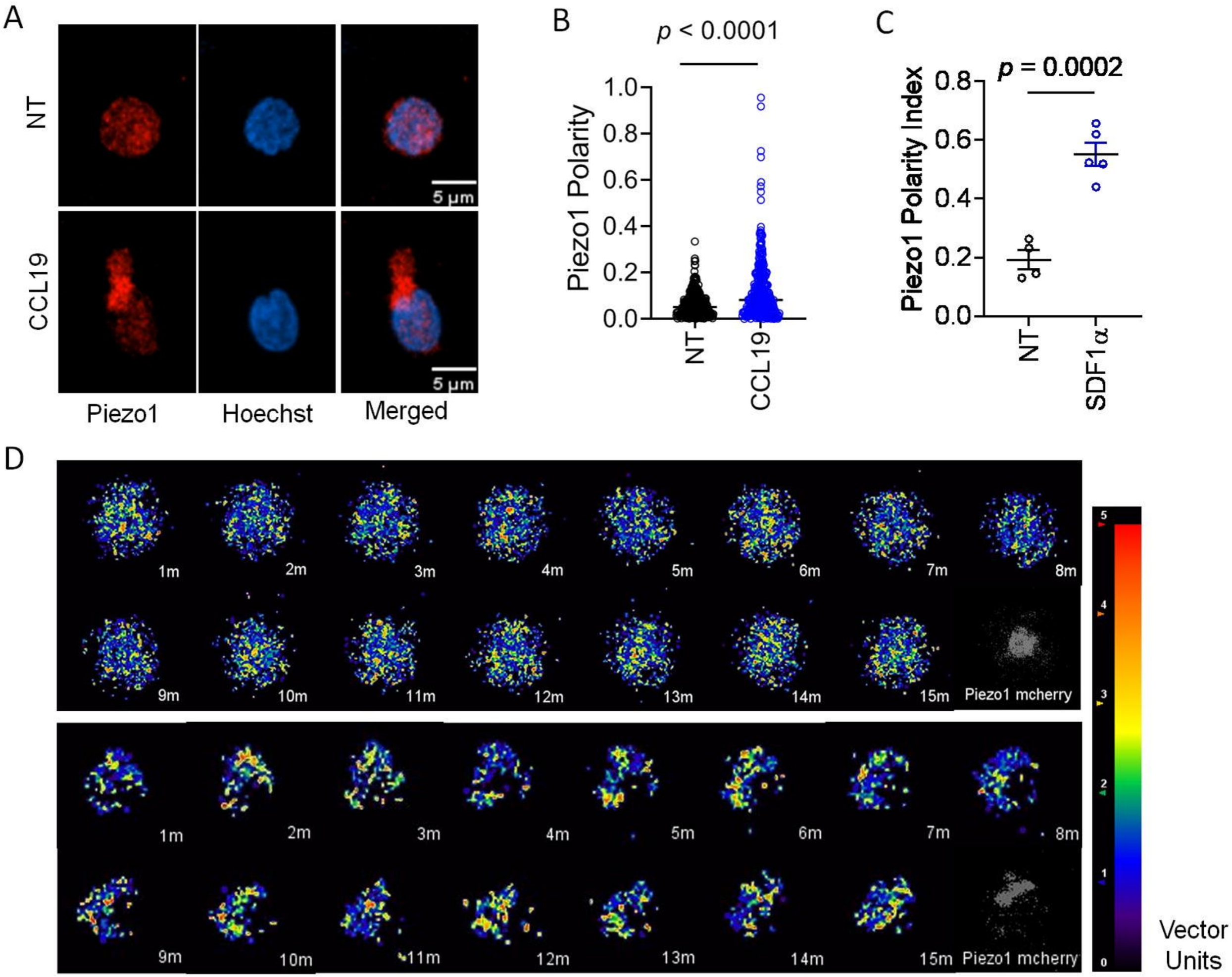
A
NT
CCL19
5 µm
5 µm
Piezo1
Hoechst
Merged
B
p < 0.0001
Piezo1 Polarity
1.0
0.8
0.6
0.4
0.2
0.0
NT
CCL19
C
p = 0.0002
Piezo1 Polarity Index
0.8
0.6
0.4
0.2
0.0
NT
SDF1α
D
1m
2m
3m
4m
5m
6m
7m
8m
9m
10m
11m
12m
13m
14m
15m
Piezo1 mcherry
5
4
3
2
1
0
Vector Units

Figure 2

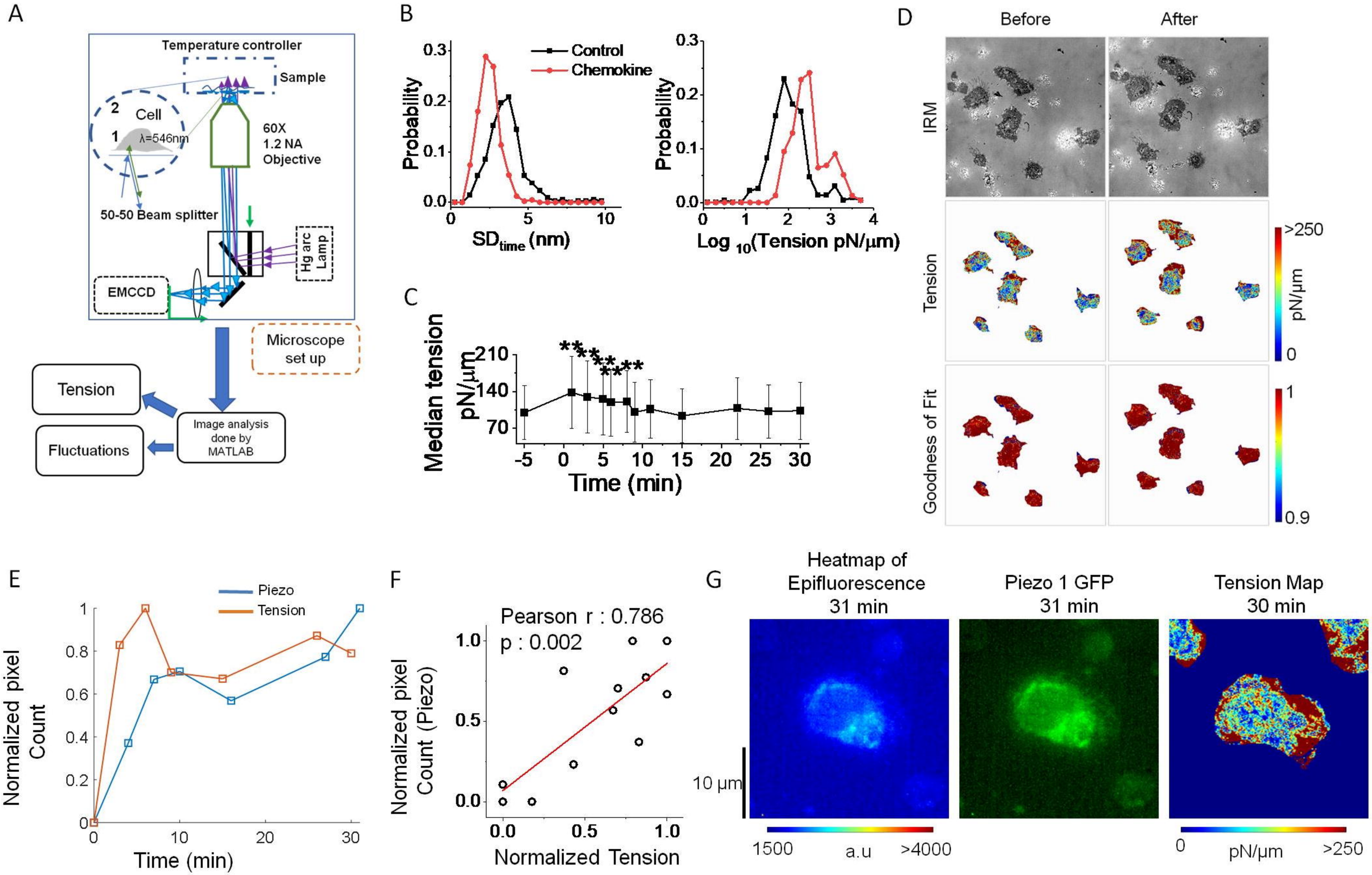
A
Temperature controller
Sample
Cell
2
1
λ=546nm
60X
1.2 NA
Objective
50-50 Beam splitter
Hg arc Lamp
EMCCD
Microscope set up
Tension
Fluctuations
Image analysis done by MATLAB
B
Control
Chemokine
Probability
SD time (nm)
Log 10(Tension pN/µm)
C
Median tension pN/µm
Time (min)
D
Before
After
IRM
Tension
Goodness of Fit
>250
pN/µm
0
1
0.9
E
Piezo
Tension
Normalized pixel Count
Time (min)
F
Pearson r : 0.786
p : 0.002
Normalized pixel Count (Piezo)
Normalized Tension
G
Heatmap of Epifluorescence 31 min
Piezo 1 GFP 31 min
Tension Map 30 min
10 µm
1500
a.u
>4000
0
pN/µm
>250

Figure 3

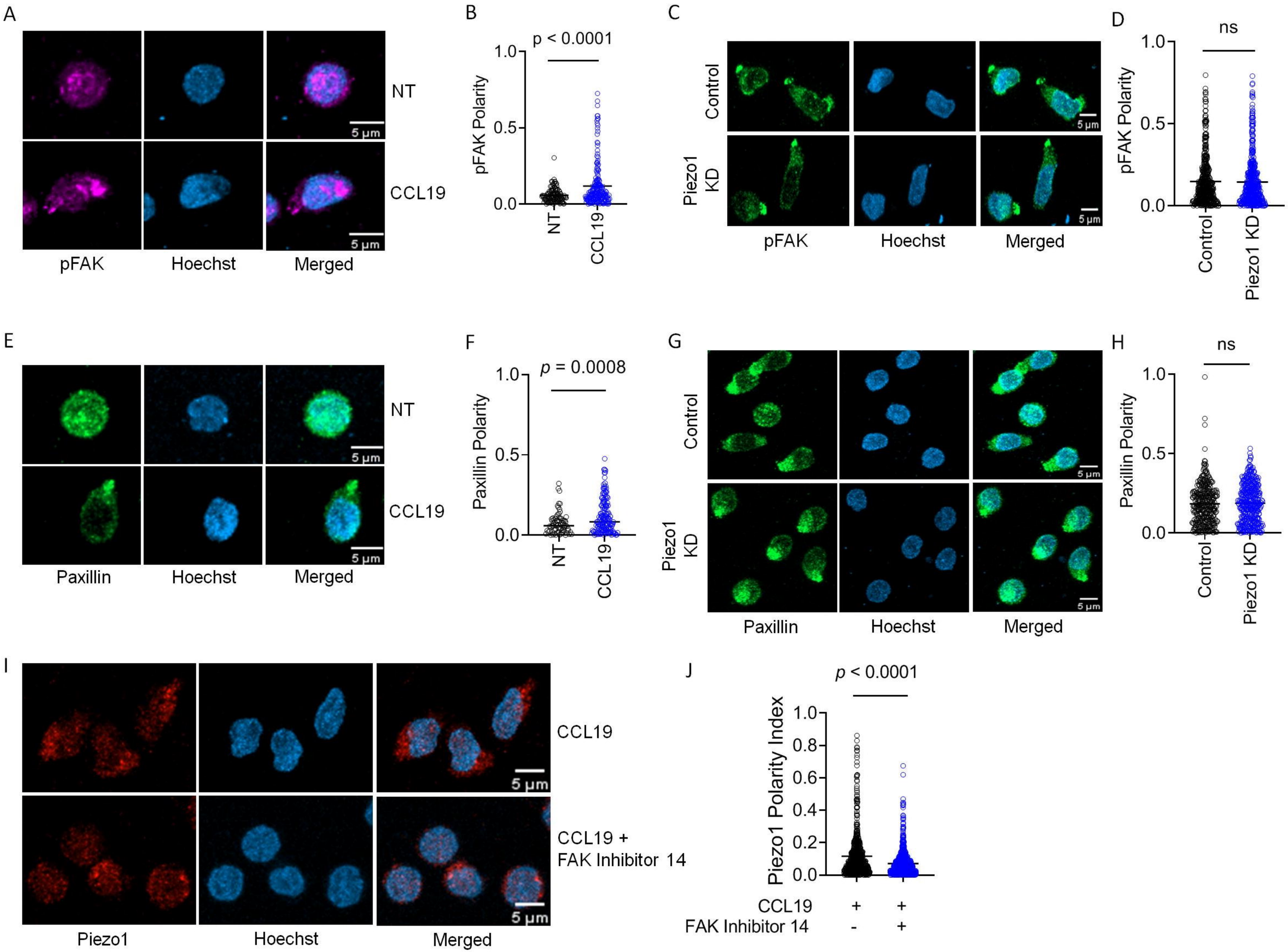
A
NT
CCL19
5 µm
pFAK
Hoechst
Merged
B
p < 0.0001
pFAK Polarity
1.0
0.5
0.0
NT
CCL19
C
Control
Piezo1 KD
5 µm
pFAK
Hoechst
Merged
D
ns
pFAK Polarity
1.0
0.5
0.0
Control
Piezo1 KD
E
NT
CCL19
5 µm
Paxillin
Hoechst
Merged
F
p = 0.0008
Paxillin Polarity
1.0
0.5
0.0
NT
CCL19
G
Control
Piezo1 KD
5 µm
Paxillin
Hoechst
Merged
H
ns
Paxillin Polarity
1.0
0.5
0.0
Control
Piezo1 KD
I
CCL19
CCL19 +
FAK Inhibitor 14
5 µm
Piezo1
Hoechst
Merged
J
p < 0.0001
Piezo1 Polarity Index
1.0
0.8
0.6
0.4
0.2
0.0
CCL19 + +
FAK Inhibitor 14 - +

Figure 4

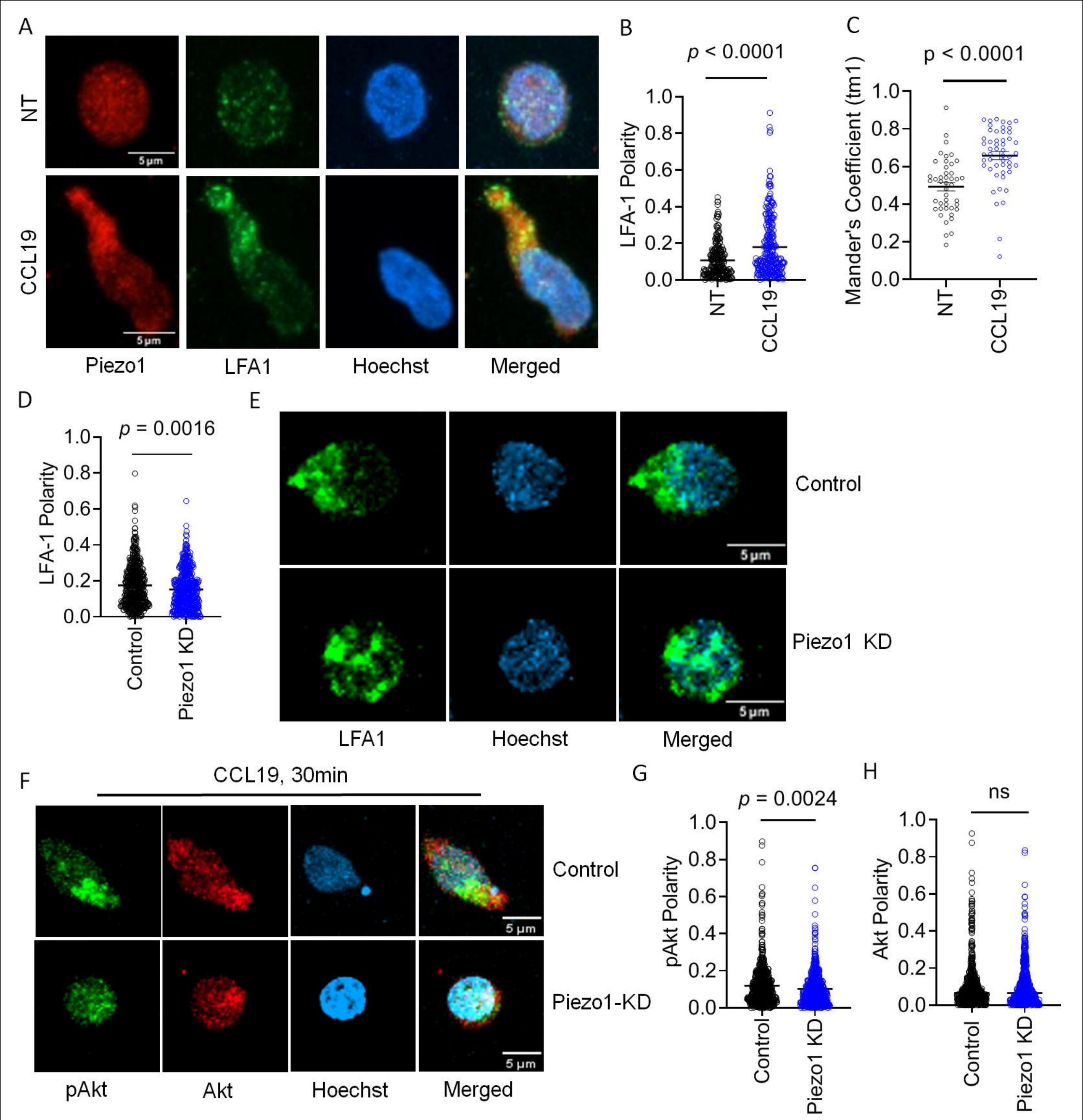
A
NT
CCL19
5 µm
Piezo1
LFA1
Hoechst
Merged
B
p < 0.0001
LFA-1 Polarity
1.0
0.8
0.6
0.4
0.2
0.0
NT
CCL19
C
p < 0.0001
Mander's Coefficient (tm1)
1.0
0.8
0.6
0.4
0.2
0.0
NT
CCL19
D
p = 0.0016
LFA-1 Polarity
1.0
0.8
0.6
0.4
0.2
0.0
Control
Piezo1 KD
E
Control
Piezo1 KD
5 µm
LFA1
Hoechst
Merged
F
CCL19, 30min
Control
Piezo1-KD
5 µm
pAkt
Akt
Hoechst
Merged
G
p = 0.0024
pAkt Polarity
1.0
0.8
0.6
0.4
0.2
0.0
Control
Piezo1 KD
H
ns
Akt Polarity
1.0
0.8
0.6
0.4
0.2
0.0
Control
Piezo1 KD

Figure 5

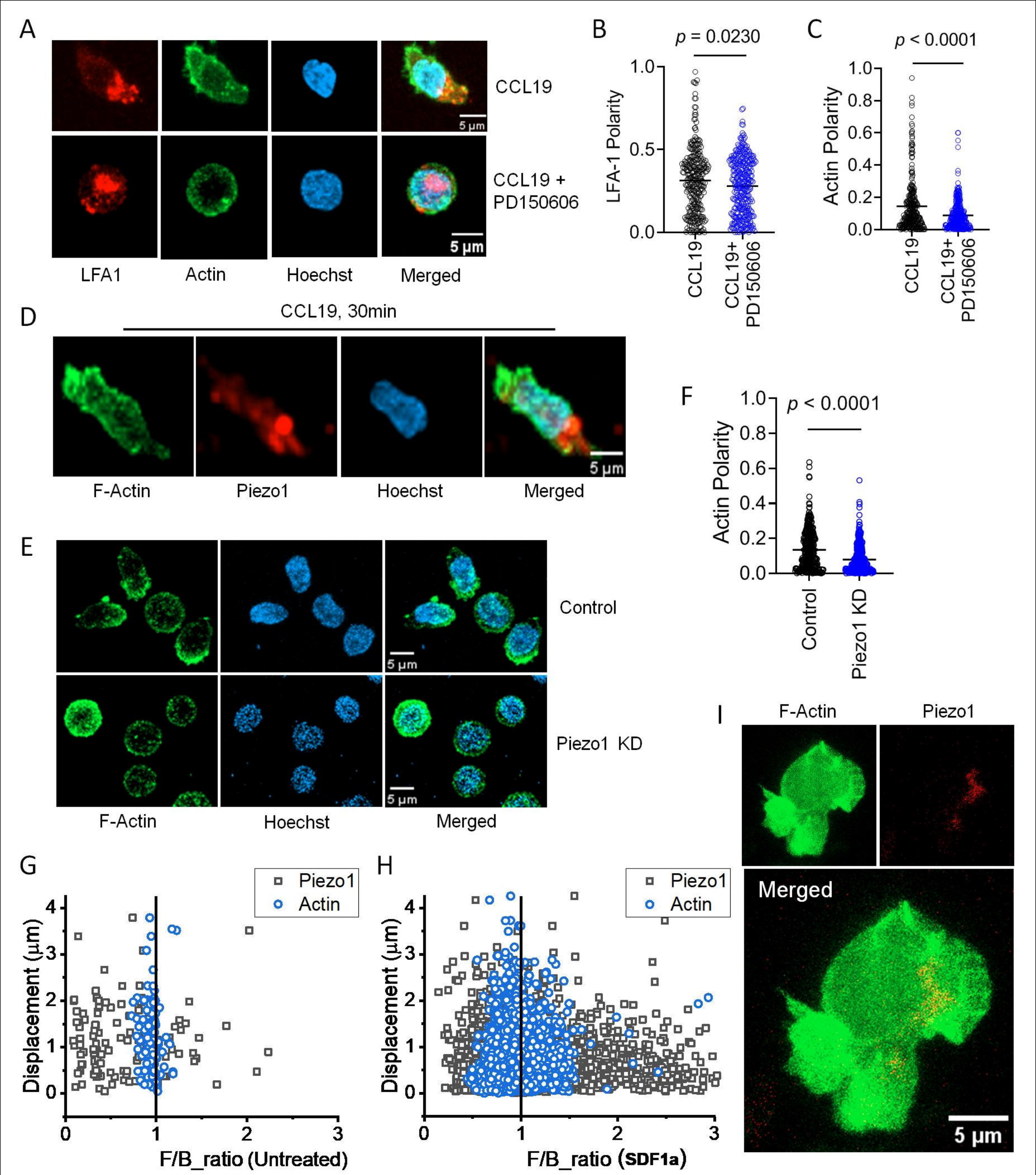
A
CCL19
CCL19 + PD150606
5 µm
LFA1
Actin
Hoechst
Merged
B
p = 0.0230
LFA-1 Polarity
1.0
0.5
0.0
CCL19
CCL19+ PD150606
C
p < 0.0001
Actin Polarity
1.0
0.8
0.6
0.4
0.2
0.0
CCL19
CCL19+ PD150606
D
CCL19, 30min
F-Actin
Piezo1
Hoechst
Merged
5 µm
E
Control
Piezo1 KD
F-Actin
Hoechst
Merged
5 µm
F
p < 0.0001
Actin Polarity
1.0
0.8
0.6
0.4
0.2
0.0
Control
Piezo1 KD
I
F-Actin
Piezo1
Merged
5 µm
G
Piezo1
Actin
Displacement (µm)
F/B_ratio (Untreated)
H
Piezo1
Actin
Displacement (µm)
F/B_ratio (SDF1a)

Figure 6

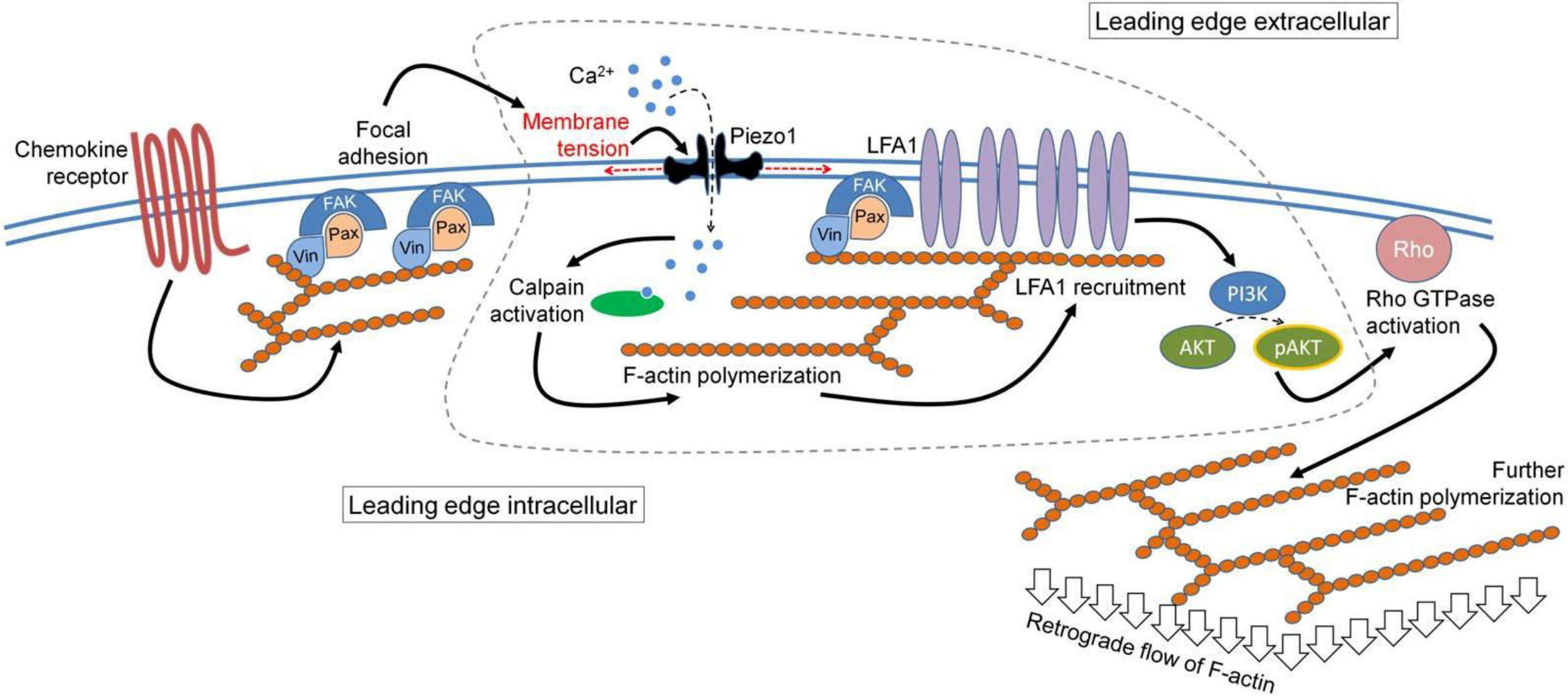
Leading edge extracellular
Ca2+
Membrane tension
Piezo1
Chemokine receptor
Focal adhesion
LFA1
FAK
Pax
Vin
FAK
Pax
Vin
FAK
Pax
Vin
Calpain activation
LFA1 recruitment
PI3K
AKT
pAKT
Rho
Rho GTPase activation
F-actin polymerization
Leading edge intracellular
Further F-actin polymerization
Retrograde flow of F-actin

Figure 7